Water Research 139 (2018) 198–207

Contents lists available at ScienceDirect

Water Research

journal homepage: www.elsevier.com/locate/watres

Pesticide degradation and export losses at the catchment scale: Insights from compound-specific isotope analysis (CSIA)

Pablo Alvarez-Zaldívar, Sylvain Payraudeau, Fatima Meite, Jeremy Masbou, Gwenaël Imfeld*

Laboratory of Hydrology and Geochemistry of Strasbourg (LHyGeS), Strasbourg University/ENGEES, CNRS, 1 rue Blessig, 67000 Strasbourg, France

ARTICLE INFO

Article history:
Received 13 December 2017
Received in revised form
23 March 2018
Accepted 26 March 2018
Available online 29 March 2018

Keywords:
CSIA
Herbicides
Monitoring
Attenuation
Mass balance

ABSTRACT

Although pesticides undergo degradation tests prior to use, determining their export, degradation and persistence under field conditions remains a challenge for water resource management. Compound specific isotope analysis (CSIA) can provide evidence of contaminant degradation extent, as it is generally independent of non-destructive dissipation (e.g., dilution, sorption, volatilization) regulating environmental concentrations. While this approach has been successfully implemented in subsurface environments, its application to pesticides in near-surface hydrological contexts at catchment scale is lacking. This study demonstrates the applicability of CSIA to track pesticide degradation and export at catchment scale and identify pesticide source areas contributing to changes in stable isotope signature in stream discharge under dynamic hydrological contexts. Based on maximum shifts in carbon stable isotope signatures ($\Delta\delta^{13}C = 4.6 \pm 0.5‰$) of S-metolachlor (S-met), a widely used herbicide, we estimate maximum degradation to have reached 96 ± 3% two months after first application. Maximum shifts in nitrogen isotope signatures were small and inverse ($\Delta\delta^{15}N = -1.3 \pm 0.6‰$) indicating potential secondary isotope effects during degradation. In combination with a mass balance approach including S-met main degradation products, total catchment non-destructive dissipation was estimated to have reached 8 ± 7% of the applied product. Our results show that CSIA can be applied to evaluate natural attenuation of pesticides at catchment scale. By providing a more detailed account of pesticide dissipation and persistence under field conditions we anticipate the contribution of pesticide CSIA to the improvement of regulatory and monitoring strategies.

1. Introduction

The widespread occurrence of micropollutants in surface and groundwater poses a threat to human water security and river biodiversity on a global scale (Vörösmarty et al., 2010). Among organic micropollutants, pesticides are one of the principal contributors to chemical risk (Malaj et al., 2014) with the potential to accumulate over decades in various environmental compartments (Sabatier et al., 2014; Rasmussen et al., 2015). Despite comprehensive exposure assessments and research evaluating toxicity, degradability and transformation products, current approaches often fail to determine where, when and how pesticide degradation occurs. This highlights the difficulties to bridge information obtained under laboratory and field conditions. Beyond regulatory testing, complementary novel management strategies (e.g., Fenner et al. (2013)) that enable monitored natural or engineered attenuation are thus warranted.

In contrast with current monitoring approaches, which are unable to distinguish among competing environmental sinks, compound specific isotope analysis (CSIA) allows for the direct quantification of pesticide degradation extent (Elsner, 2010). During chemical transformation, lighter isotopes (e.g., ^{12}C) exhibit lower activation energy, generally resulting in faster reaction times relative to their heavier counterparts (e.g., ^{13}C). This leads to an enrichment of the heavier isotopologues in the non-degraded pesticide fraction remaining in environmental samples (Elsner, 2010). The resulting average isotope value (e.g., $\delta^{13}C$) of the non-degraded fraction can then be used to quantify degradation by following the Rayleigh distillation equation (Rayleigh, 1896). Research on legacy contaminants (Sherwood Lollar et al., 2001; Hunkeler et al., 2008) and nitrate pollution (Nestler et al., 2011;

* Corresponding author.
E-mail address: imfeld@unistra.fr (G. Imfeld).

https://doi.org/10.1016/j.watres.2018.03.061
0043-1354/

Fenech et al., 2012), have shown CSIA to be a valuable complementary line of evidence to demonstrate degradation, persistence and source identification at various temporal and spatial scales. Akin to these approaches, application of CSIA to pesticides relies on the ability to monitor changes in stable isotope composition between source(s) and outlet to quantify the extent of (bio)chemical conversion at the catchment scale.

This study evaluated the feasibility of carbon-based CSIA as a first characterization approach for monitoring pesticide fate at catchment scale under dynamic hydrological and rainfall-runoff conditions. The use of carbon-based CSIA to evidence natural attenuation is well established for legacy compounds in contaminated sites (Thullner et al., 2009) and thus may be considered as a relevant approach to monitor pesticide degradation and export across distinct hydrological events. However, principal limitations to the applicability of pesticide CSIA at catchment scale are the occurrence of low (sub-$\mu g/L$) environmental concentrations, which lead to challenges in analyte extraction and quantification under field contexts (Schreglmann et al., 2013; Elsner and Imfeld, 2016). While changes in $\delta^{13}C$ tend to be smaller in larger molecules (Elsner, 2010), the higher contribution of carbon atoms to the total molecular mass may allow for the collection of more environmental samples at or above quantification limits. This is of particular interest when seeking detailed characterization of rainfall-runoff events requiring high-resolution data made possible by flow-proportional sampling strategies. An important trade-off however, is the limitations in sample volumes that may be achieved due to automatic sampler unit capacities, therefore challenging catchment-scale CSIA studies during discharge periods where environmental concentrations are low. In this respect, although multi-element CSIA may also be desirable to further improve characterization (Elsner and Imfeld, 2016), its feasibility will be challenged by the sampling window where quantification limits can be achieved.

By implementing a CSIA high resolution monitoring strategy, the objectives of this study were then to (i) demonstrate the validity of pesticide CSIA as a complementary line of evidence for quantifying degradation extent under field conditions; (ii) infer off-site losses due to non-destructive dissipation (e.g., dilution, volatilization, sorption) and; (iii) demonstrate applicability of pesticide CSIA under shifting hydrological regimes. To address these objectives, the study tracked S-metolachlor (S-met) in an agricultural headwater catchment (47 ha) during one growing season, a period where degradation and off-site transfer risk is most relevant. As a well characterized and widely used herbicide (i.e., 4.2% of global pesticide use) that is frequently detected in groundwaters (Fenner et al., 2013), S-met is a relevant model compound for establishing a first effort of catchment-wide pesticide CSIA characterization.

2. Materials and methods

2.1. Catchment description

The 47 ha catchment is located 30 km north-east of Strasbourg (Bas-Rhin, France; 48 47 19,56 N; 7 35 2,27 E) and has been previously described by Lefrancq et al., (2017b). The mean catchment slope is 6.7 ± 4.7% with altitude ranging between 190 and 230 m. Catchment water flows in ditches to a 50 cm diameter pipe at a single outlet. Roads represent 3.5% of the catchment surface and in 2016, 88% was arable land, from which sugar beet (70%) and corn (18%) were the principal crops sown between mid-March and late April (Fig. 1A).

Overall, the soil characteristics indicate little variability. Surface soil samples (0–20 cm, n = 30) and soil profiles (2 m, n = 6) have a grain size distribution of clay 30.8 ± 3.9%, silt 61.0 ± 4.5%, and sand 8.5 ± 4.2%. The main soil type is Haplic Cambisol Calcaric Siltic and Cambisol Eutric Siltic on hillsides (north and south) and Cambisol Colluvic Eutric Siltic in the central valley. Soil characteristics were $CaCO_3$ = 1.1 ± 1.6%; organic matter = 2.2 ± 0.3%; pH = 6.7 ± 0.8; total soluble phosphorus = 0.11 ± 0.04 g/kg, and CEC = 15.5 ± 1.3 cmol/kg. A compacted layer (plough pan) was observed at a depth between 20 and 30 cm.

2.2. Hydrological conditions

A summary of the catchment hydrological conditions during the study period, between April 1st and June 28*th* 2016, is presented in Table 1. The summary data provided includes mean daily rainfall (P), mean rainfall intensity (P_{int}), total rainfall (P_{tot}), mean daily reference evapotranspiration (ETP), mean daily temperature (T), mean daily discharge normalized by the total catchment area (Q), the time of concentration (T_C) and the percent of days in a month were rainfall occurred (% Wet Days). The time of concentration (T_C) is defined as the time between the start of rainfall minus evapotranspiration and the resulting peak discharge (Gericke and Smithers, 2014). Although subsurface travel times for this catchment range from 6 to 12 months (Lutz et al., 2017), T_C values decreased from 2.2 to 0.5 h (Table 1). Soil crust development was generally observed across the catchment after around 100 mm of cumulative rainfall. A reduction in the soil infiltration capacity due to observed crusting and the progressive increase in mean daily and total monthly rainfall likely contributed to the observed decrease in the catchment's T_C.

2.3. Top soil and water collection

Top soil (1 cm) concentrations and $\delta^{13}C$ were determined by weekly sampling on three transects across the catchment. Transects where selected to account for variability of moisture conditions, drainage characteristics and to maximize the number of plots where S-met was applied (Fig. 1). A digital Elevation Model (DEM), at 2 m resolution, was used to obtain local slopes and to estimate the topographical wetness index (TWI) [−] (Fig. 1B), which quantifies the influence of topography on soil moisture such that (Beven and Kirby, 1979):

$$TWI = ln\left(\frac{a}{tan(b)}\right) \quad (1)$$

where a is the upslope area draining through a certain point per unit contour length and $tan(b)$, the local slope in radians.

Discharge at the catchment outlet was continuously measured by a Doppler flow-meter (2150 Isco, Lincoln, Nebraska, USA) with discharge precision of 3%. Water was collected by flow proportional sampling using a refrigerated automatic sampler with a total capacity of 3.96 L divided into 12 glass vials each of 330 mL (Isco Avalanche, Lincoln, Nebraska, USA). A predefined discharged volume based on the seasonal rainfall intensity expected for April (50 m^3), May (100 m^3) and June (150 m^3) was chosen allowing for 36 aliquots of 110 mL each per week. Water samples were then combined into composite samples according to hydrograph characteristics (base-flow, rising and/or falling limb), yielding one to four samples weekly of volumes ≥ 990 mL.

2.4. Farmer surveys

S-met was applied on three different dates, on March 25 (plots: 5, area: 14.9 ha), April 14 (plots: 8, area: 8.2 ha) and on May 25 (plots: 5, area: 5.9 ha) (Table 2 and Fig. 5C). Farmers used one of two Syngenta product formulations, Mercantor Gold (area applied: 97%)

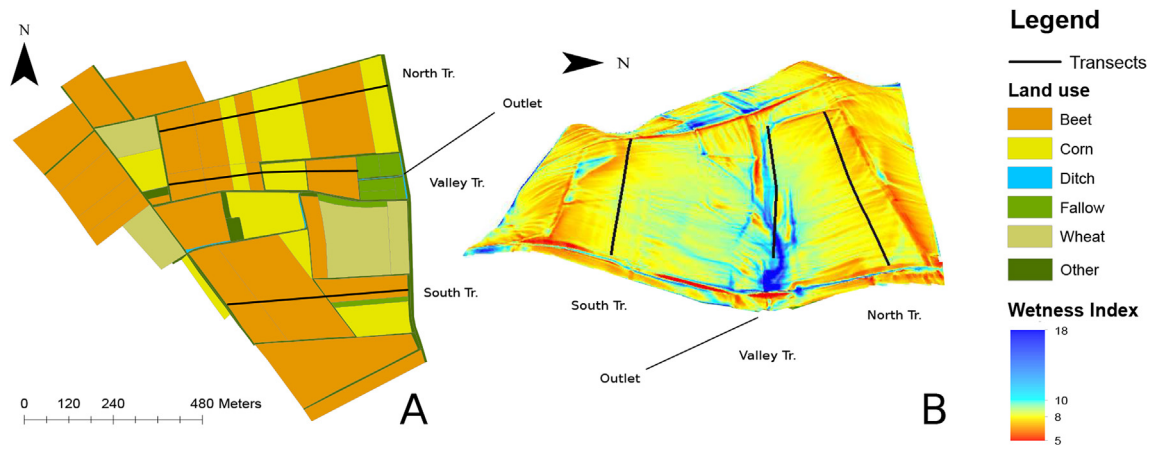

Fig. 1. Catchment land-use (A) and topographical wetness index (B) (Beven and Kirby, 1979). The wetness index is computed with SAGA in QGIS 2.18 using the Topographical Wetness Index (TWI) tool with options "local upstream area" and the slope map in radians according to equation (1).

Table 1
Catchment Hydrological Conditions (mean ± 1σ, total or %) between April 1*st* and June 28*th*, 2016.

	P (mm/d)	P_{int} (mm/h)	P_{tot} (mm)	ETP (mm/d)	T (°C)	Q (mm/d)	T_C (h)	% Wet Days
April	2.7±4.6	1.1±0.9	82.2	2.2±0.8	9.1±2.9	0.6±0.6	2.2±1.8, n = 9	67%
May	4.6±7.1	1.7±2.8	136.8	3.1±1.2	14±3.2	0.9±1.3	0.9±0.6, n = 13	63%
June	4.8±7.0	1.8±3.1	145.6	3.7±1.2	17.6±2.9	1.2±1.2	0.5±0.2, n = 14	80%

Note: Abbreviations pertain to mean daily rainfall (P), mean rainfall intensity (P_{int}), total rainfall (P_{tot}), mean daily reference evapotranspiration (ETP), mean daily temperature (T), mean daily discharge normalized by the total catchment area (Q), the time of concentration (T_C) and the percent of days in a month were rainfall occurred (% Wet Days).

Table 2
Applied mass (Kg) of active S-met per transect by date.

Date	North	Valley	South
25 March 2016	5.1	1.6	11.1
14 April 2016	8.0	1.8	2.9
29 May 2016	7.2	2.4	0.0
Total	20.3	5.8	14.0

or Dual Gold (area applied: 3%). Technical dosage specifications were 0.6 and 1.2 L/ha, with pure product S-met concentrations of 960 g/L and 915 g/L, respectively. Signatures were obtained *via* dilution in Milli-Q water and followed the same solid-phase extraction (SPE) procedure described below for environmental waters. Initial $\delta^{13}C$ (-32.2 ± 0.5‰, n = 17) and $\delta^{15}N$ (1.9 ± 0.5‰, n = 17) were obtained from pure product and tractor tank dilutions. Pure product and tractor tank dilutions were not significantly different (Table S4).

2.5. Pesticide extraction and quantification

S-met and its degradation products metolachlor ethane sulfonic acid (MESA) and metolachlor oxanilic acid (MOXA) were extracted from soil and outlet water samples (Supporting Information (SI), section *IV. Pesticide extraction*). Water samples were extracted by solid-phase extraction (SPE) using SolEx C18 cartridges (Dionex®, Sunnyvale, CA, USA) and an AutoTrace 280 SPE system (Dionex®) as described previously (Elsayed et al., 2014), and quantified by GC-MS/MS (S-met) and by LC-MS/MS (MESA and MOXA), as described previously (Elsayed et al., 2014). Pesticide extraction and purification for soils were adapted from Ivdra et al., (2014) and Anastassiades et al. (2003). Environmental quantification limits for the soil samples were 0.001, 0.1, 0.1 µg/g dry weight (d.w.) for S-met, MOXA and MESA with an analytical uncertainty of 16%, 40% and 8% respectively.

2.6. Isotope analysis

The carbon and nitrogen isotope composition of S-met was analysed by adapting a previously described protocol (Elsayed et al., 2014) and further detailed in the SI. The GC-C-IRMS system consisted of a TRACE™ Ultra Gas Chromatograph (ThermoFisher Scientific) coupled *via* a GC IsoLink/Conflow IV interface to an isotope ratio mass spectrometer (DeltaV Plus, ThermoFisher Scientific). The reproducibility of triplicate measurements was ≤ 0.2‰ (1σ) for $\delta^{13}C$ and ≤ 0.5‰ (1σ) for $\delta^{15}N$. The carbon and nitrogen isotope ratios are reported in δ notation in parts per thousand [‰] relative to the V-PDB standard for carbon and Air standard for nitrogen, according to:

$$\delta^{13}C_{sample} \text{ or } \delta^{15}N_{sample}\left[‰\right] = \left(\frac{R_{sample} - R_{standard}}{R_{standard}}\right)\cdot 1000 \qquad (2)$$

where R_{sample} and $R_{standard}$ are the ratios $\frac{^{13}C}{^{12}C}$ or $\frac{^{15}N}{^{14}N}$ of sample and standard, respectively. Based on GC-IRMS linearity tests, the minimum peak amplitudes needed for accurate $\delta^{13}C$ and $\delta^{15}N$ measurements were established as about 300 mV and 200 mV, respectively (Fig. S6). These signals correspond to 10 ng of carbon and 20 ng of nitrogen injected on column.

2.7. Soil degradation experiments

To derive a carbon isotope enrichment factor (ε_{lab}) for S-met, signatures and remaining concentrations were obtained from soil microcosm experiments and conducted over a period of 200 days over a set of temperatures (20 and 30 °C) and moisture conditions (20 and 40% volumetric water content). Derivation of ε_{lab} with eq. (3) was then used to infer field degradation extent based on isotope signatures measured in field samples and eq. (15). Microcosms consisted of 20 g air-dried soil obtained from the catchment and were spiked to environmental concentrations (5.0 µg/g soil) in

20 mL crimp glass vials, with silicone/natural PTFE caps (Interchim®, France). To maintain aerobic conditions while limiting water loss and avoiding contamination, a 0.2 μm syringe filter (Rotilabo®, Carl Roth®, France) was mounted on a syringe tip and installed through a vial cap (Fig. S7). To distinguish sorption from microbial degradation, and to determine whether isotope fractionation could arise due to non-destructive dissipation (i.e., sorption) or abiotic degradation (i.e., hydrolysis), half of the soil samples were three-times autoclaved in glass bottles and stored in the dark at room temperature for 12 h between each autoclave run. Sacrificial sampling was conducted in triplicate at days 1, 10, 50, 100 and 200. Fractionation extent and dissipation kinetics are provided in Table S5.

Abiotic controls showed no significant isotope fractionation, confirming insignificant fractionation associated to sorption and hydrolysis (Fig. S8, SI section *VII Degradation experiments*). A carbon S-met enrichment (ε_{lab}) was derived from living microcosm experiments by following the classical Rayleigh equation (Rayleigh, 1896):

$$\frac{\delta^{13}C_t + 1}{\delta^{13}C_0 + 1} = f^{\,\varepsilon} \tag{3}$$

where $f = [\text{S-met}]_t/[\text{S-met}]_0$, is the remaining fraction of S-met at time t.

2.8. Predictive calculations

Predictive approaches required computing remaining masses based on farmer surveys and estimating degradation extent according to median (21 d), minimum (7.6 d) and maximum (37.6 d) half-lives ($t_{1/2}$) reported for S-met (PPDB, 2009). Calculation in soils where computed according to:

$$M_{tot,t} = M_{tot,t_0}\left(\frac{1}{2}\right)^{\frac{t}{t_{1/2}}} \tag{4}$$

where M_{tot} is the total catchment mass at time t.

2.9. Mass balance calculations

Soils. Pesticide mass along a catchment's transect area $M_{Tr,t}$ [μg] is given by:

$$M_{Tr,t} = C_{Tr,t} \cdot \rho_{b_0} \cdot A_{Tr} \cdot D \tag{5}$$

were C_{Tr} is the dry weight S-met soil concentration [$\mu g/g$ *soil dry wt*] on transect Tr at time t, A_{Tr} is the associated transect area [m^2] and D is sampling depth (1 *cm*). A homogeneous bulk density ($\rho_{b_0} = 0.99\ g/cm^3$) was assumed based on sample measurements obtained across the catchment.

Transect signature and pesticide mass were then used to compute bulk signatures across the catchment ($\delta^{13}C_{bulk}$) and given by:

$$\delta^{13}C_{bulk,t} = \sum_{Tr=1}^{TR=3} \frac{M_{Tr,t}}{M_{tot,t}} \delta^{13}C_{Tr,t} \tag{6}$$

were $\delta^{13}C_{Tr}$ is the S-met carbon isotope signature in transect Tr. The total catchment mass, M_{tot} [μg], at time t is obtained by adding eq. (5) for all three transects.

Outlet. Outlet loadings (OL) [μg] where calculated based on flow proportional samples given by:

$$OL_{ws} = C_{ws} \int_{t}^{\Delta t} V(t)dt \tag{7}$$

where C the concentration [$\mu g/L$] of water sample ws and V [L] is discharge over the sample time interval Δt [h]. Transformation product (TP) loadings were expressed in S-met mass equivalence (MEQ_{S-met}) [μg] such that:

$$MEQ_{S-met} = MOXA \cdot \left(\frac{mw_{S-met}}{mw_{MOXA}}\right) + MESA \cdot \left(\frac{mw_{S-met}}{mw_{MESA}}\right) \tag{8}$$

where mw is the molar mass of each species measured at the outlet. MB errors associated to missed sampling intervals were corrected by linear interpolation between measured sample concentrations.

2.10. CSIA and open-system Rayleigh calculations

The Rayleigh equation assumes that $f = C_t/C_0$ reflects solely reduction in concentrations due to degradation and should thus be expressed as $f_{degradation}$. Accounting for dilution processes, the remaining fraction that is measured in the field sample becomes then f_{total} (Van Breukelen, 2007):

$$f_{total} = f_{degradation} \cdot f_{dilution} \tag{9}$$

$$f_{dilution} = \frac{1}{F} \tag{10}$$

where F is the number of times the sampled volume has become diluted. F can be calculated if ε_{lab} is known such that:

$$F = e^{(\Delta*/\varepsilon_{lab} - ln f_{total})} \tag{11}$$

$$\Delta* = 1000 \cdot ln\left(\frac{10^{-3}\delta^{13}C_t + 1}{10^{-3}\delta^{13}C_0 + 1}\right) \tag{12}$$

where $\Delta*$ is the isotopic shift of the measured sample at time t.

The total fraction remaining (f_{total}) was estimated based on the concentration (C_t) measured along a transect (Tr) at any given time t relative to the cumulative initial concentration (C_{Tr_0}) [$\mu g/g$ *soil*] after a timely application (a_t) and given by:

$$C_{Tr,t_0} = \frac{\sum_{a=1}^{A} M_{Tr,a_t}}{A_{Tr} \cdot D \cdot \rho_{b_0}} \tag{13}$$

where, M_{Tr,a_t} [μg S-met] is the total mass applied on transect Tr due to application a at time t (Table 2), the total plot area [m^2] associated to the transect (A_{Tr}), which is proportional to sampling points along a transect, the sampling depth (D) [m] and the initial soil bulk density (ρ_{b_0}) [g/m^3]. Measured concentrations ($C_{Tr,t}$) and remaining fractions ($f_{total} = C_{Tr,t}/C_{Tr,t_0}$) across time per transect are detailed in the SI, tables S6, S7 and S8.

The carbon isotope enrichment factor (ε_{lab}), derived from closed microcosm degradation experiments under mixed aerobic and anaerobic conditions (section 2.7), was used to quantify field degradation ($B\%$). Degradation was then determined from the remaining fraction associated to degradation ($f_{degradation}$) such that (Hunkeler et al., 2008):

$$f_{degradation} = \left(\frac{\delta^{13}C_t + 1}{\delta^{13}C_0 + 1}\right)^{1/\varepsilon_{lab}} \quad (14)$$

$$B\% = \left(1 - f_{degradation}\right) \cdot 100 \quad (15)$$

To obtain the relative contribution of degradation and dilution (e.g., off-site export, sorption), the open-system Rayleigh equation (Van Breukelen, 2007) was adapted for tops soils. The relative contribution of dilution and degradation to concentration decrease is represented by the factor ratio D*/B*, where dilution (D*) and breakdown (B*) factors are given by:

$$D^* = \frac{lnf_{dilution}}{lnf_{total}} \quad (16)$$

$$B^* = \frac{lnf_{degradation}}{lnf_{total}} = 1 - D^* \quad (17)$$

and where $D^* \geq 0$ and $0 \leq B^* \leq 1$. For example, if $D^*/B^* = 0$ ($D^* = 0$; $B^* = 1$), the concentration decline is solely due to degradation, while if $D^*/B^* = 1$ ($D^* = B^* = 0.5$), the contribution of each processes to the logarithmic concentration decrease is equal (Van Breukelen, 2007).

3. Results and discussion

3.1. S-met degradation and carbon isotope fractionation in top soils

S-met $\delta^{13}C$ signatures and concentrations were obtained on a weekly basis on catchment top soils (1 cm) from April to June 2016. Soil concentrations negatively correlated with changes in isotope shift ($\Delta\delta^{13}C$) across time ($r = -0.7$, $P < 0.001$) (Fig. 2A). To allow quantification of field degradation extent, microcosm degradation experiments were conducted (section 2.7) to derive a carbon isotope enrichment factor ($\varepsilon_{lab} = -1.5 \pm 0.5‰$, $R^2 = 0.87$, $P < 0.001$). Assuming a reactive position at the C-Cl bond, this corresponds to an apparent kinetic isotope effect ($AKIE_C$) ranging from 1.02 to 1.03 (eq. S(5)) compatible with S_N2 ($AKIE_C = 1.03–1.07$) type substitution reactions and reductive cleavage of C-Cl bonds ($AKIE_C = 1.02–1.03$) (Elsner et al., 2005). Although $\delta^{15}N$ values were also measured, derivation of a nitrogen isotope enrichment was not possible due to high matrix interference effects in soils leading to significant uncertainty in measured signals ($\geq 1‰$).

To estimate the error extent that could arise from derivation of enrichment values in the field, a carbon isotope field enrichment (ε_{field}) was also derived based on top soil samples and compared against ε_{lab} (Fig. 2B). Due to open system conditions, the field derived enrichment is expected to underestimate ε_{lab} (i.e., be less negative) and consequently lead to an overestimation of degradation extent. As expected, a catchment-wide ε_{field} underestimated ε_{lab} (Fig. 2B). However, this underestimation was small, likely reflecting S-met high sorptive properties and indicating good transferability of ε values between laboratory and field conditions for this compound.

Abiotic controls for S-met degradation experiments showed no significant isotope shift, which indicated no fractionation associated to sorption and agreement with previous results (Imfeld et al., 2014; Kopinke et al., 2017) (section 2.7, SI, section VII., Fig. S8 and Table S5). Field measurements of top soil and outlet signatures also support this observation, as fractionation extent in water samples taken both near application periods and towards the end of the season generally remains equivalent or slightly lower relative to top soil samples (Fig. 4). Based on a multiple lines of evidence approach derived from the combined CSIA, mass balance (MB) and predictive calculations in the following section, attribution of degradation extent to photochemical degradation is likely to be small (< 5%), if not negligible. Indeed, carbon isotope effects associated to photochemical degradation in aqueous solutions of aniline substructures have been reported to be negligible under indirect photolysis (Ratti et al., 2015a) and nearly insensitive to inverse at environmental pH (Ratti et al., 2015b). If inverse fractionation where to be of relevance for this case, CSIA biodegradation estimations would therefore be regarded as conservative. Nevertheless, photochemical degradation is not expected (PPDB, 2009) or may be low when incorporated into the top soil (Kochany and Maguire, 1994; EXTOXNET, 1996; Wilson and Mabury, 2000; Dimou et al., 2005), which is supported by similar lab and field enrichment values as well as by comparisons of non-degraded fractions *vs.* remaining mass measured in top soils (see following section, Fig. 3. B *vs.* C).

3.2. Validation of the CSIA approach

The value of CSIA as a complementary monitoring tool was assessed by comparing information derived from both MB accounts and reported half-life ranges for S-met (7.6–49.5 days) (European Commission, 2004; PPDB, 2009; Wu et al., 2011). Results indicate good agreement between CSIA, MB and predictive calculations, which emphasizes the validity of the CSIA approach (Fig. 3). Based

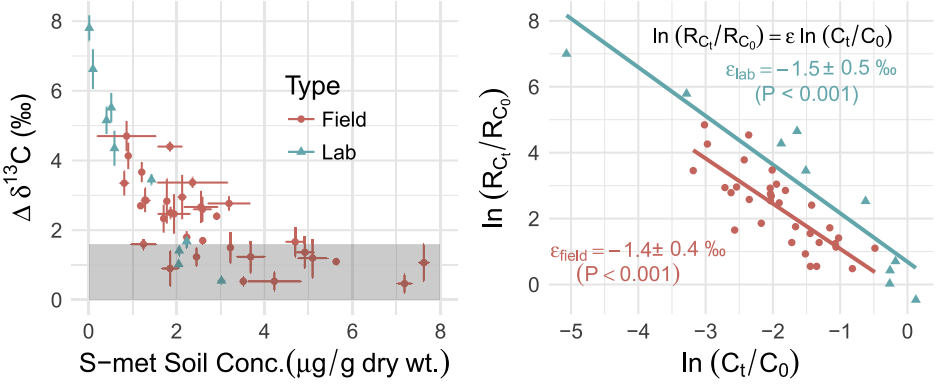

Fig. 2. S-met carbon isotope shift ($\Delta\delta^{13}C = \delta^{13}C_t - \delta^{13}C_0$) *vs.* concentration in transect soils, where $\delta^{13}C_0 = -32.2 \pm 0.5‰$. Error bars account for error propagation (e.p.) across $\pm 1\sigma$ (standard deviation) of initial product and $\pm 1\sigma$ from sample signatures (eq. S(3)). Analytical uncertainty ($1\sigma \leq \pm 0.5‰$) incorporates both accuracy and reproducibility of $n \geq 3$ measurements. The shaded area represents the minimum shift below which degradation should not be concluded (i.e. uncertainty limit) due to maximum analytical uncertainties, sample error uncertainties, and minor shifts in the soil extraction method (eq. S(1)).

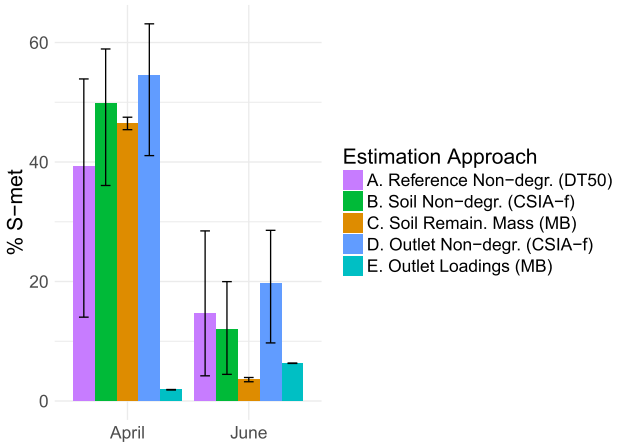

Fig. 3. Estimation of remaining S-met relative to the cumulative applied mass (%). Estimation of remaining fractions were based on the referenced typical field half-life, with error bars representing referenced half-life ranges (A); the non-degraded fraction ($CSIA - f$) calculated from isotope signatures in soils (B) and outlet waters (D), with error bars corresponding to 95% confidence intervals (±0.4‰) of S-met ε_{lab}; the remaining mass based on measured soil sample concentrations and standard deviations (C); and the total fraction of discharged mass in S-met molar equivalents for MESA and MOXA (outlet loadings), with error bars representing the cumulative standard deviation (E).

on CSIA estimations in soils (Fig. 3B), S-met was degraded by 50% and 88% by the end of April (32 days after 1*st* application) and June (82 days after 1*st* application), respectively. Propagation errors in catchment degradation extent associated to statistical variation of CSIA input parameters was estimated to be $|\Delta B| = 19\%$ in April and 9% in June (Thullner et al., 2012). Relative to the CSIA approach, single first-order degradation predictions (Fig. 3A, eq. (4)) based on a field half-life of 21 days (PPDB, 2009), slightly overestimated degradation in April ($|\Delta B| = 10\%$) and were nearly equivalent in June ($|\Delta B| = 4\%$). Overestimation in April was likely due to low spring temperatures and largest degradation rates associated to higher concentrations when computed by the single first-order rate model. Comparison of a half-life of 34 days obtained during the degradation experiment (i.e., based on catchment soils) further indicates that lower field degradation rates may also be attributed to soil characteristics. Nevertheless, although both methods provide approximately equivalent estimations, CSIA was able to reduce the uncertainty margins relative to the reported half-life ranges (i.e., see error bars across methods in Fig. 3A *vs.* Fig. 3B).

Soil MB accounts during April and June (Fig. 3C) indicated remaining fractions of 46% and 4%, with only 0.1% and 0.2% of S-met reaching the outlet, respectively. Comparing information from CSIA (Fig. 3B) and MB approaches (Fig. 3C), inferred top soil non-destructive losses (e.g., sorption, infiltration, run-off and volatilization) were estimated to have reached 8% of the applied product. Plant uptake was considered to be negligible, as no correlation was found between remaining mass and crop growth (from 0 to 40 cm) or surface cover (from 0 to 100%) (Lefrancq et al., 2017b). Although S-met is considered to be a non-volatile compound (VP = 1.73 mPa) (Corbin et al., 2006), based on environmental conditions (e.g., Prueger et al., 2005) and model based calculations (Lefrancq et al., 2017b) we estimate volatilization to have accounted for ≤ 5% of the applied product.

Comparison of the type of information that can be derived from CSIA and MB approaches at the outlet illustrates a further advantage of tracking pesticide fate using CSIA. By tracking parent and major TPs, direct information regarding source zone degradation extent cannot be appreciated, as mass balances cannot be closed due to long subsurface travel times within the catchment, the potential for further TP degradation and difficulties in determining sorption extent without numerical modeling. On the other hand, the use of CSIA generally provided a good approximation of the degradation extent observed in source top soils (Fig. 3B *vs.* 3D), as tracking S-met, carries information of its degradation extent independently of the total loads exported. In this respect, CSIA presents an opportunity as a complementary line of evidence to the rapidly developing capabilities of high-resolution mass spectrometry for target and non-target analyses of pesticide TPs (e.g., Kern et al., 2009). By providing information on the maximum degradation achieved by parent compounds, CSIA may thus contribute to monitoring programs seeking to develop chemical risk assessments requiring more accurate MB accounts.

3.3. CSIA-based monitoring under dynamic hydrological regimes

To determine whether CSIA could be implemented at reduced effort and be of relevance, for example, in larger catchments contexts, we evaluated whether a catchment-wide assessment could be conducted by monitoring discharge water at the catchment outlet. To do so, we compared linear trends of isotope fractionation in bulk top soils against stream discharge at the catchment outlet across time (Fig. 4). Bulk top soils are computed by eq. (6) and provide a more accurate representation of the catchment wide signature evolution by taking mass balances into account. An approximately equivalent and general increase in $\Delta\delta^{13}C$ above uncertainty ranges (i.e., shaded area) was observed across time for bulk soils and waters. However, linear trends indicate that without top soil information, outlet trends would have underestimated catchment-wide degradation by $\Delta B \approx 8\%$ towards the end of the season (mid-June). This underestimation was however, likely related to an increase in variability of isotope signatures in source soils following a late season application on May 25*th* (Fig. 4) and observed at the outlet due to significant changes in hydrological conditions taking place in late May and June (see SI section III for detailed analysis of hydrological variability).

To identify potential source contribution leading to isotope variability, the relative contribution of degradation and dilution to concentration decrease, given by the factor ratio D*/B*, in transect soils was estimated across time (Van Breukelen, 2007, section 2.10). Although mass flux contributions from each area would be necessary for a quantitative source apportionment (i.e., *via* end-member analysis), D*/B* ratios in top soils may be used as qualitative source indicators for outlet $\delta^{13}C$ and S-met concentration variability. Weekly D*/B* calculations (Tables S7, S8 and S9) considered two enrichment scenarios based on the derived $\varepsilon_{lab} = -1.5$‰ and on $\varepsilon_{max} = -1.9$‰. The latter considers a conservative maximum kinetic isotope effect of KIE = 1.03 (C-Cl bond) expected for S_N2 reactions (Elsner et al., 2005), and approximates degradation conditions observed during the microcosm experiment for saturated moisture levels (Table S5, $\theta = 40\%$).

A comparison between rainfall, discharge, S-met concentrations in outlet and soils, and D*/B* ratios across time in Fig. 5 shows how D*/B* ratios were highest (Fig. 5D) shortly after rainfall events, when outlet concentrations exceeded the seasonal trends (Fig. 5B). Median D*/B* ratios for the north, valley and south transects (Table 3) indicate that dilution was more significant shortly after applications, with each transect showing dilution to be as important as degradation (D*/B* ≥ 1) at least once early in the season (April to mid-May). Further inference of D*/B* ratios indicates that dilution along the steeper slopes and better drained soils of the north transect continued to be of more importance during the late season relative to other transects, where drainage was poor. Low D*/B* ratios along the south during the late season indicate potential contributions to outlet concentrations of lesser importance.

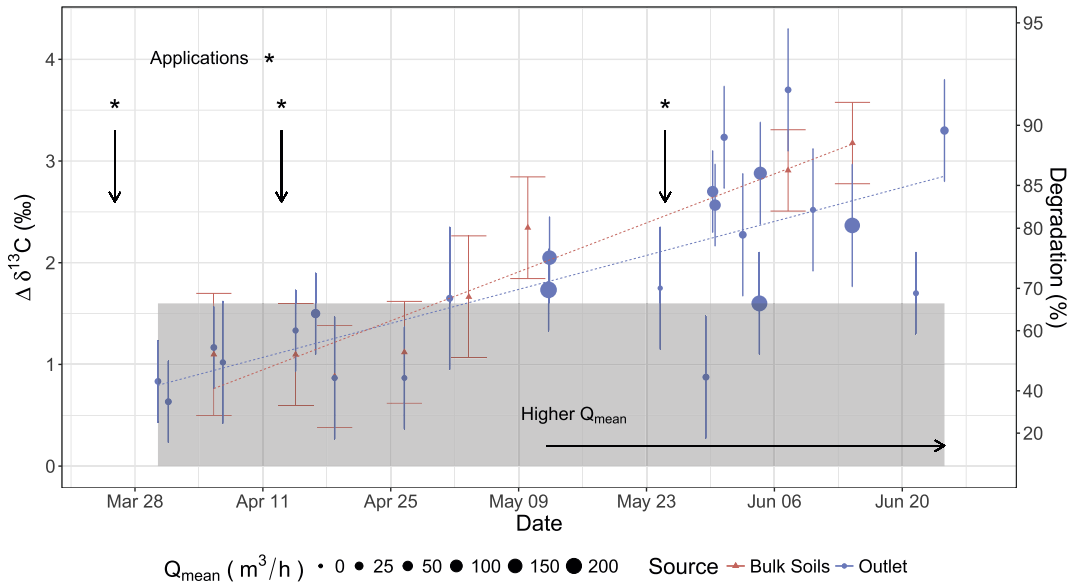

Fig. 4. S-met carbon isotope shift ($\Delta\delta^{13}C$) across time in bulk soils and outlet waters with vertical arrows indicating application dates ($\delta^{13}C_0 = -32.2\pm0.5‰$). Fitted linear models ($\Delta\delta(t) = mt$) for outlet signatures ($R^2_{out} = 0.5$) and bulk soils ($R^2_{soil} = 0.9$) *vs.* days (t) after first application illustrate similar trends in time, despite an increase in variability for outlet signatures during May and June. Error bars account for error propagation (e.p.) across $\pm1\sigma$ (standard deviation) of initial product and $\pm1\sigma$ from sample signatures (eq. S(3)). Analytical uncertainty ($1\sigma \leq \pm0.5‰$) incorporates both accuracy and reproducibility of $n \geq 3$ measurements. The shaded area represents the minimum shift below which degradation should not be concluded (i.e. uncertainty limit) due to maximum analytical uncertainties, sample error uncertainties, and minor shifts in the soil extraction method (eq. S(1)). Degradation extent (%) shown on secondary y-axis is obtained from $\Delta\delta^{13}C$ transformations based on ε_{lab} (eqs. (14) and (15)).

This is supported by significant differences ($P < 0.05$, Kruskal-Wallis) in $\delta^{13}C$ observed between outlet and the south transect during the late season (Fig. 6), indicating that the south transect was unlikely responsible for outlet isotope variability within this period. Finally, two major rainfall-runoff events, with outlet S-met concentrations exceeding late-season trends, can be appreciated on May 29*th* and June 25*th*. With respect to the former event, no appreciable influence can be observed on the north and south transects. However, D*/B* ratios along the valley, which received a late season application on May 25*th*, were significantly higher (D*/B* = 0.8–1.2) relative to its overall median values (D*/B* = 0.1–0.5), likely indicating this transect as the main source leading to drops in outlet $\delta^{13}C$ (and S-met concentration increase) during this event. A comparable observation can also be made for the latter (June 25*th*) event. However, this time the source of outlet variability shortly after the rainfall event may be most likely attributed to the north transect, where increases in outlet concentrations (Fig. 5B) and a drop in outlet $\delta^{13}C$ (Fig. 4) coincide with an increase in D*/B* ratios (D*/B* = 1.1–1.7) measured on June 28*th* (Fig. 5D) for this transect relative to median values (D*/B* = 0.6–1.0).

Although these results alone cannot provide quantitative insights of the contribution of pesticide from each area to outlet, comparison of degradation extents to remaining masses can be used to estimate export losses from top soils. However, values of B* > 1 along the valley and in the late season along the south, indicate an overestimation of degradation extent based on the overall ε_{lab}. During these periods (e.g., where moisture levels were likely high in these areas), estimation based on the more conservative ε_{max} may thus be more appropriate, as observed during the microcosm experiment (Table S5, $\theta = 40\%$). A comparison of end of season (June 21*th* - 28*th*) remaining mass ($RM_{north} = 2\%$; $RM_{valley} = 13\%$; $RM_{south} = 4\%$) against degradation extents ($B_{north} = 85\%$; $B_{valley} = 84\%$; $B_{south} = 94\%$), yielded non-destructive losses of ≈ 16% along the north and valley transects *vs.* only 2% in the south. While the low relative losses observed in the south also support a minor role for volatilization (Lefrancq et al., 2017a) and photodegradation, the valley and north transect accounted for 91% of total export losses (2.8 kg of S-met or 7% of the total applied product), despite representing only 50% of the catchment area. This highlights the potential value of CSIA approaches to identify critical areas of degradation and off-site export, even where complete MB accounts may not be available.

3.4. Perspectives for pesticide CSIA applications at catchment scale

Detailed soil and sub-event CSIA data allowed us to determine the evolution of pesticide degradation extent and export losses across the catchment. Additional insights on mechanisms of bond cleavage however, could have been obtained using multi-element CSIA of nitrogen, hydrogen or chlorine (Wu et al., 2018). Unfortunately, the ability to implement multi-element isotope analysis was reduced by current limitations in CSIA quantification from environmental samples. Indeed, seeking sub-event information to better understand the catchment's primary pesticide transport processes limited our ability to collect sufficient volumes during each forcing event and also derive a nitrogen based high-resolution data set. Namely, given the small contribution of nitrogen (≈ 5%), hydrogen (≈ 8%), and chlorine (≈ 12%) to the molar mass of a S-met molecule and the amount required of each element for analysis (about 20 ng on column for nitrogen and hydrogen and 10 ng for chlorine) significantly larger environmental concentrations would have been required to achieve the study objectives (i.e., a combined mass balance and carbon-based CSIA account under a high-resolution monitoring strategy). For example, at minimum environmental concentrations of ≈ 1 $\mu g/L$ the extraction from about 56, 40 and 8 L, respectively for either nitrogen, hydrogen or chlorine, would have been required (Fig. S2).

Despite these challenges, additional concentration steps allowed quantification of nitrogen isotope fractionation ($\delta^{15}N$) for sub-event samples with highest concentrations (n = 7). These samples are associated to periods near application dates and during one major event. Maximum nitrogen isotope shifts were inverse

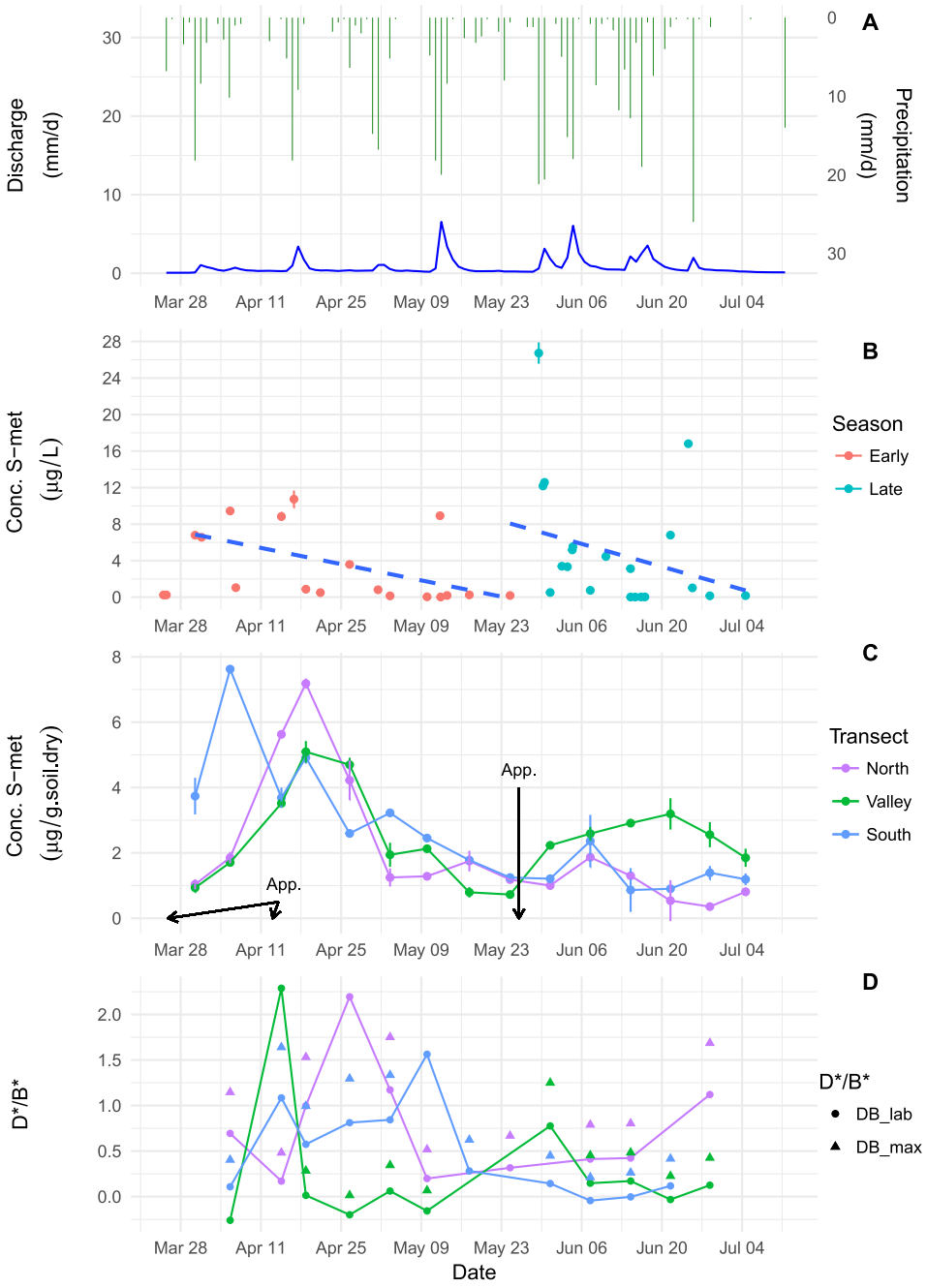

Fig. 5. Hydrological forcing and catchment response to pesticide applications across the growing season. Error bars represent $\pm 1\sigma$. Rainfall and discharge at the outlet (mm/d) (A), outlet concentrations before (early season) and after (late season) second pesticide application $(\mu g/L)$ (B); composite transect soil concentrations $(\mu g/g\ dry\ weight)$ and pesticide application (App.) dates (C); and D*/B* ratios based on $\varepsilon_{lab} = 1.5‰$ and $\varepsilon_{max} = -1.9‰$ (D).

but small ($\Delta\delta^{15}N = -1.3\pm0.6‰$, Fig. S5), indicating potential secondary isotope effects during biodegradation (Elsner and Imfeld, 2016). Attempts to construct laboratory and field nitrogen enrichment values from soils however, were not possible due to high matrix interference effects leading to significant uncertainty in measured $\delta^{15}N$ values ($>1‰$). In this respect, enrichment cultures isolated from relevant soils should prove crucial in the interpretation of field studies implementing multi-element pesticide CSIA.

Based on the observed limitations associated to the high-resolution approach followed in this study, catchment scale characterization campaigns implementing micropollutant CSIA should therefore account for a trade-off in information objectives inherent to pesticide CSIA analytical limitations and near-surface hydrological contexts. Namely, (i) improving understanding of pesticide fate during periods of high transfer risk, and (ii) seeking an evaluation of competing degradation processes across catchment compartments. Under the former objective (i), a high-resolution sampling scheme involving carbon-based CSIA should enable quantification of pesticide degradation across multiple events and catchment areas, as it was achieved in this study. However, when attempting to achieve the latter objective (ii), low-flow conditions may preclude obtaining information associated to base-flow components and therefore an understanding of long travel time degradation characteristics within the catchment. Evidently, similar challenges are

Table 3
Degradation (B%), breakdown factors (B*) & D*/B* ratios for $\varepsilon_{lab} = -1.5‰$ and $\varepsilon_{max} = -1.9‰$ along the North, Valley and South transects.

Transect	B_{lab} (%)	B_{max} (%)	B^*_{lab} (−)	B^*_{max} (−)	D^*/B^*_{lab} (−)	D^*/B^*_{max} (−)
North						
Early Season	53.1	45.0	0.6	0.5	0.7	1.1
Late Season	85.4	78.1	0.7	0.6	0.4	0.8
Overall	74.4	66.2	0.6	0.5	0.6	1.0
Valley						
Early Season	56.2	59.6	0.9	0.8	0.1	0.3
Late Season	82.1	75.6	0.9	0.7	0.2	0.5
Overall	80.8	73.3	0.9	0.7	0.1	0.5
South						
Early Season	61.0	52.4	0.6	0.4	0.8	1.3
Late Season	93.1	87.9	0.9	0.7	0.1	0.3
Overall	64.4	60.3	0.6	0.6	0.6	0.6

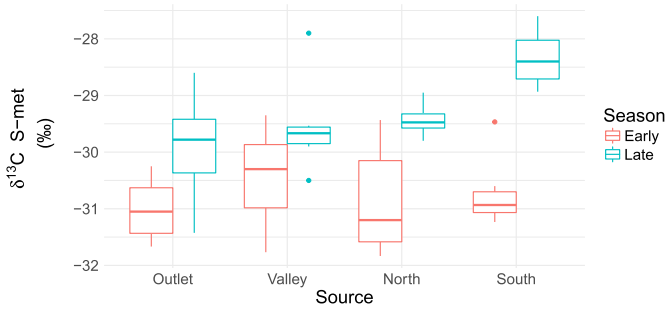

Fig. 6. Distribution of carbon isotope signatures in outlet and soil transects across early and late season groups. Initial pesticide product isotope signature: $\delta^{13}C_0 = -32.2 \pm 0.5‰$, n = 11.

to be expected under multi-element CSIA approaches. Therefore, monitoring strategies seeking subsurface compartment characterization, may be advised to target narrower sampling time-frames, particularly if MB accounts are of lesser priority relative to multi-element CSIA information.

4. Conclusion

This study evaluated the feasibility of carbon-based CSIA approaches as a tool to monitor pesticide fate at catchment scale. Comparison of three information sources (i.e., CSIA, MB and reported half-life ($t_{1/2}$) ranges) demonstrated the validity of pesticide CSIA as a complementary line of evidence for quantifying degradation under dynamic hydrological and rainfall-runoff conditions. The CSIA approach improved our understanding of pesticides fate by delineating the primary catchment areas regulating degradation (88%) and export losses (8%). Comparison of MB and CSIA approaches showed that degradation extent evolution was consistent between outlet and catchment-wide top soils, demonstrating the monitoring applicability of CSIA methods despite shifting hydrological regimes. It should be noted however, that due to potential artifacts in soil extraction methods, a minimum shift of $\Delta\delta^{13}C > 2‰$ ($\approx$ 75% degradation) was considered before any conservative conclusion on degradation extent could be established. Based on its ability to quantify degradation independently of TPs and to delineate critical source areas, CSIA may thus be considered as a valuable complementary tool to identify and monitor chemical risk at catchment scale. Further efforts seeking to implement high-resolution CSIA approaches at greater scales should be supported by adequate characterization of dominant transport pathways regulating critical source areas. During periods of relatively low flow however, and where MB information is of lower priority, non-proportional (e.g., manual) sampling efforts may nevertheless be of interest to successfully characterize long-term discharge. In this respect, modeling of slow catchment response behavior may facilitate the selection of minimum sampling volumes and the design of extraction protocols required to achieve higher resolution of multi-dimensional CSIA.

Competing financial interest

The authors declare no competing financial interest.

Acknowledgements

P. Alvarez-Zaldívar was supported by an *Initiatives d'excellence* (IDEX) fellowship. F. Meite was supported by a fellowship of the Alsace Region and the Rhine-Meuse Water Agency (Projet PACOV). J. Masbou was supported by a fellowship of the Graduate Academy SERIOR of the European INTERREG V program Upper Rhine. The authors wish to acknowledge S. Wisselmann, M. Levasseur, C. Wiegert, and B. Guyot for support in sampling and analysis and B. Droz for helpful comments on the article's structure and organization. We would also like to thank the Alteckendorf farmers for their collaboration during the field study.

Supplementary Information

Supplementary data related to this article can be found at https://doi.org/10.1016/j.watres.2018.03.061.

References

Anastassiades, M., Lehotay, S.J., Štajnbaher, D., Schenck, F.J., 2003. Fast and easy multiresidue method employing acetonitrile extraction/partitioning and "dispersive solid-phase extraction" for the determination of pesticide residues in produce. J. AOAC Int. 86, 412–431.

Beven, K.J., Kirby, M.J., 1979. A physically based, variable contributing area model of basin hydrology. Hydrol. Sci. Bull. 24, 43–69. https://doi.org/10.1080/02626667909491834. http://www.tandfonline.com/doi/abs/10.1080/02626667909491834.

Corbin, M., Eckel, W., Ruhman, M., Spatz, D., Thurman, N., Gangaraju, R., Kuchnicki, T., Mathew, R., Nicholson, I., 2006. NAFTA Guidance Document for Conducting Terrestrial Field Dissipation studies https://www.epa.gov/pesticide-science-and-assessing-pesticide-risks/nafta-guidance-document-conducting-terrestrial-field{\#}IC.

Dimou, A.D., Sakkas, V.a., Albanis, T.a, 2005. Metolachlor photodegradation study in aqueous media under natural and simulated solar irradiation. J. Agric. Food Chem. 53, 694–701. https://doi.org/10.1021/jf048766w.

Elsayed, O.F., Maillard, E., Vuilleumier, S., Nijenhuis, I., Richnow, H.H., Imfeld, G., 2014. Using compound-specific isotope analysis to assess the degradation of chloroacetanilide herbicides in lab-scale wetlands. Chemosphere 99, 89–95. https://doi.org/10.1016/j.chemosphere.2013.10.027. https://doi.org/10.1016/j.chemosphere.2013.10.027.

Elsner, M., 2010. Stable isotope fractionation to investigate natural transformation mechanisms of organic contaminants: principles, prospects and limitations. J. Environ. Monit. : JEM 12, 2005–2031. https://doi.org/10.1039/c0em00277a. http://www.ncbi.nlm.nih.gov/pubmed/21038038.

Elsner, M., Imfeld, G., 2016. Compound-specific isotope analysis (CSIA) of micro-pollutants in the environment - current developments and future challenges. Curr. Opin. Biotechnol. 41, 60–72. https://doi.org/10.1016/j.copbio.2016.04.014.

Elsner, M., Zwank, L., Hunkeler, D., Schwarzenbach, R.P., 2005. A new concept linking observable stable isotope fractionation to transformation pathways of organic pollutants. Environ. Sci. Technol. 39, 6896–6916. https://doi.org/10.1021/es0504587. https://doi.org/10.1021/es0504587.

European Commission, 2004. Review Report for the Active Substance S-Metolachlor. Technical Report. European Commission Health & Consumer Protection Directorate-General. http://ec.europa.eu/food/plant/pesticides/eu-pesticides-database/public/?event=activesubstance.ViewReview{\&}id=381.

EXTOXNET, 1996. Extoxnet. Extension toxicology network. Pesticide information profiles. http://extoxnet.orst.edu/pips/metolach.htm.

Fenech, C., Rock, L., Nolan, K., Tobin, J., Morrissey, A., 2012. The potential for a suite of isotope and chemical markers to differentiate sources of nitrate contamination: a review. Water Res. 46, 2023–2041. https://doi.org/10.1016/j.watres.2012.01.044. https://doi.org/10.1016/j.watres.2012.01.044.

Fenner, K., Canonica, S., Wackett, L.P., Elsner, M., 2013. Evaluating pesticide

degradation in the environment: blind spots and emerging opportunities. Science 341, 752–758. https://doi.org/10.1126/science.1236281 http://www.ncbi.nlm.nih.gov/pubmed/23950532{%}5Cnhttp://www.sciencemag.org/cgi/doi/10.1126/science.1236281.

Gericke, O.J., Smithers, J.C., 2014. Review of methods used to estimate catchment response time for the purpose of peak discharge estimation. Hydrol. Sci. J. 59, 1935–1971. https://doi.org/10.1080/02626667.2013.866712. http://www.tandfonline.com/doi/abs/10.1080/02626667.2013.866712.

Hunkeler, D., Meckenstock, R.U., Lollar, B.S., Schmidt, T.C., Wilson, J.T., 2008. A guide for assessing biodegradation and source identification of organic ground water contaminants using compound specific isotope analysis (CSIA). USEPA publication Epa 600/R, pp. 1–82 papers2://publication/uuid/FD7382F3-6250-449D-9B49-9B7F20B8F1E6{%}5Cnwww.epa.gov/ada{%}5Cnpapers2://publication/uuid/4D3218BF-F0A7-44F8-8C93-0401674D7357, doi:EPA/600/R-08/148, arXiv:600/R-08/148.

Imfeld, G., Kopinke, F.D., Fischer, A., Richnow, H.H., 2014. Carbon and hydrogen isotope fractionation of benzene and toluene during hydrophobic sorption in multistep batch experiments. Chemosphere 107, 454–461. https://doi.org/10.1016/j.chemosphere.2014.01.063. https://doi.org/10.1016/j.chemosphere.2014.01.063.

Ivdra, N., Herrero-Martín, S., Fischer, A., 2014. Validation of user- and environmentally friendly extraction and clean-up methods for compound-specific stable carbon isotope analysis of organochlorine pesticides and their metabolites in soils. J. Chromatogr. A 1355, 36–45. https://doi.org/10.1016/j.chroma.2014.06.014.

Kern, S., Fenner, K., Singer, H.P., Schwarzenbach, R.P., Hollender, J., 2009. Identification of transformation products of organic contaminants in natural waters by computer-aided prediction and high-resolution mass spectrometry. Environ. Sci. Technol. 43, 7039–7046. https://doi.org/10.1021/es901979h.

Kochany, J., Maguire, R.J., 1994. Sunlight photodegradation of metolachlor in water. J. Agric. Food Chem. 42, 406–412. https://doi.org/10.1021/jf00038a032.

Kopinke, F.D., Georgi, A., Imfeld, G., Richnow, H.H., 2017. Isotope fractionation of benzene during partitioning - Revisited. Chemosphere 168, 508–513. https://doi.org/10.1016/j.chemosphere.2016.11.029. http://linkinghub.elsevier.com/retrieve/pii/S0045653516315648.

Lefrancq, M., Dijk, P.V., Jetten, V., Schwob, M., Payraudeau, S., 2017a. Improving runoff prediction using agronomical information in a cropped, loess covered catchment. Hydrol. Process. 31, 1408–1423. https://doi.org/10.1002/hyp.11115.

Lefrancq, M., Payraudeau, S., Benoit, G., Millet, M., Imfeld, G., 2017b. Degradation and transport of the chiral herbicide S-metolachlor at the catchment scale: combining observation scales and analytical approaches. Environ. Sci. Technol. 51, 13231–13240.

Lutz, S.R., van der Velde, Y., Elsayed, O.F., Imfeld, G., Lefrancq, M., Payraudeau, S., van Breukelen, B.M., 2017. Pesticide fate at catchment scale: conceptual modelling of stream CSIA data. Hydrol. Earth Syst. Sci. Discuss. 21, 5243–5261. https://doi.org/10.5194/hess-2017-202. https://www.hydrol-earth-syst-sci-discuss.net/hess-2017-202/.

Malaj, E., von der Ohe, P.C., Grote, M., Kühne, R., Mondy, C.P., Usseglio-Polatera, P., Brack, W., Schäfer, R.B., 2014. Organic chemicals jeopardize the health of freshwater ecosystems on the continental scale. Proc. Natl. Acad. Sci. U.S.A. 111, 9549–9554. https://doi.org/10.1073/pnas.1321082111.

Nestler, A., Berglund, M., Accoe, F., Duta, S., Xue, D., Boeckx, P., Taylor, P., 2011. Isotopes for improved management of nitrate pollution in aqueous resources: review of surface water field studies. Environ. Sci. Pollut. Control Ser. 18, 519–533. https://doi.org/10.1007/s11356-010-0422-z.

PPDB, 2009. The Pesticide Properties Database. Developed by the Agriculture & Environment Research Unit (AERU). University of Hertfordshire, funded by UK national sources and the EU-funded FOOTPRINT project (FP6-SSP-022704). https://sitem.herts.ac.uk/aeru/index.htm.

Prueger, J.H., Gish, T.J., McConnell, L.L., McKee, L.G., Hatfield, J.L., Kustas, W.P., 2005. Solar radiation, relative humidity, and soil water effects on metolachlor volatilization. Environ. Sci. Technol. 39, 5219–5226. https://doi.org/10.1021/es048341q.

Rasmussen, J.J., Wiberg-Larsen, P., Baattrup-Pedersen, A., Cedergreen, N., McKnight, U.S., Kreuger, J., Jacobsen, D., Kristensen, E.A., Friberg, N., 2015. The legacy of pesticide pollution: an overlooked factor in current risk assessments of freshwater systems. Water Res. 84, 25–32. https://doi.org/10.1016/j.watres.2015.07.021. https://doi.org/10.1016/j.watres.2015.07.021.

Ratti, M., Canonica, S., McNeill, K., Bolotin, J., Hofstetter, T.B., 2015a. Isotope fractionation associated with the indirect photolysis of substituted anilines in aqueous solution. Environ. Sci. Technol. 49, 12766–12773. https://doi.org/10.1021/acs.est.5b03119.

Ratti, M., Canonica, S., McNeill, K., Bolotin, J., Hofstetter, T.B., 2015b. Isotope fractionation associated with the photochemical dechlorination of chloroanilines. Environ. Sci. Technol. 49, 9797–9806. https://doi.org/10.1021/acs.est.5b02602.

Rayleigh, L.S., 1896. Theoretical considerations respecting the separation of gases by diffusion and similar processes. Phil. Mag. 42, 493–498. https://doi.org/10.1080/14786449608620944. https://doi.org/10.1080/14786449608620944.

Sabatier, P., Poulenard, J., Fanget, B., Reyss, J.L., Develle, A.L., Wilhelm, B., Ployon, E., Pignol, C., Naffrechoux, E., Dorioz, J.M., Montuelle, B., Arnaud, F., 2014. Long-term relationships among pesticide applications, mobility, and soil erosion in a vineyard watershed. Proc. Natl. Acad. Sci. U.S.A. 111, 15647–15652. https://doi.org/10.1073/pnas.1411512111. http://www.ncbi.nlm.nih.gov/pubmed/25313074.

Schreglmann, K., Hoeche, M., Steinbeiss, S., Reinnicke, S., Elsner, M., 2013. Carbon and nitrogen isotope analysis of atrazine and desethylatrazine at submicrogram per liter concentrations in groundwater. Anal. Bioanal. Chem. 405, 2857–2867. https://doi.org/10.1007/s00216-012-6616-0.

Sherwood Lollar, B., Slater, G.F., Sleep, B., Witt, M., Klecka, G.M., Harkness, M., Spivack, J., 2001. Stable carbon isotope evidence for intrinsic bioremediation of tetrachloroethene and trichloroethene at Area 6, Dover Air Force Base. Environ. Sci. Technol. 35, 261–269. https://doi.org/10.1021/es001227x.

Thullner, M., Centler, F., Richnow, H.H., Fischer, A., 2012. Quantification of organic pollutant degradation in contaminated aquifers using compound specific stable isotope analysis ??? Review of recent developments. Org. Geochem. 42, 1440–1460. http://www.sciencedirect.com/science/article/pii/S0146638011002944. https://doi.org/10.1016/j.orggeochem.2011.10.011.

Thullner, M., Richnow, H.h, Fischer, A., 2009. characterization and quantification of in situ biodegradation of groundwater contaminants using stable isotope fractionation analysis: advantages and limitations. In: Gallo, D., Mancini, R. (Eds.), Environmental and Regional Air Pollution, vol. 1. Nova Science Publishers, Inc. (chapter 2).

Van Breukelen, B.M., 2007. Quantifying the degradation and dilution contribution to natural attenuation of contaminants by means of an open system Rayleigh equation. Environ. Sci. Technol. 41, 4980–4985.

Vörösmarty, C.J., McIntyre, P.B., Gessner, M.O., Dudgeon, D., Prusevich, A., Green, P., Glidden, S., Bunn, S.E., Sullivan, C.A., Liermann, C.R., Davies, P.M., 2010. Global threats to human water security and river biodiversity. Nature 468, 555–561. https://doi.org/10.1038/nature09549 arXiv:arXiv:1011.1669v3. http://www.nature.com/doifinder/10.1038/nature09549.

Wilson, R.I., Mabury, S.a, 2000. Photodegradation of metolachlor: isolation, identification, and quantification of monochloroacetic acid. J. Agric. Food Chem. 48, 944–950. https://doi.org/10.1021/jf990618w.

Wu, L., Chládková, B., Lechtenfeld, O.J., Lian, S., Schindelka, J., Herrmann, H., Richnow, H.H., 2018. Characterizing chemical transformation of organophosphorus compounds by 13 C and 2 H stable isotope analysis. Sci. Total Environ. 615, 20–28. https://doi.org/10.1016/j.scitotenv.2017.09.233. http://linkinghub.elsevier.com/retrieve/pii/S0048969717325846.

Wu, X., Li, M., Long, Y., Liu, R., 2011. Effects of adsorption on degradation and bioavailability of metolachlor in soil. Soil Sci. Plant Nutr. 11, 83–97. https://doi.org/10.4067/S0718-95162011000300007. http://www.scielo.cl/scielo.php?pid=S0718-95162011000300007.